Activity-dependent maturation of prefrontal gamma oscillations sculpts cognitive performance

Sebastian H. Bitzenhofer[1,*,§], Jastyn A. Pöpplau[1], Mattia Chini[1], Annette Marquardt[1] & Ileana L. Hanganu-Opatz[1,*]

[1] Developmental Neurophysiology, Institute of Neuroanatomy, University Medical Center Hamburg-Eppendorf, Hamburg, Germany
[§]Current address: Center for Neural Circuits and Behavior, Department of Neurosciences, University of California, San Diego, La Jolla, CA, USA.

* Corresponding author: Ileana L. Hanganu-Opatz
hangop@zmnh.uni-hamburg.de
Falkenried 94, 20251 Hamburg, Germany

Sebastian Bitzenhofer
sebbitz@zmnh.uni-hamburg.de
Falkenried 94, 20251 Hamburg, Germany

4 figures
Words: Abstract 70, Main 1883, 39 references
Supplementary Material: Methods, Supplementary Fig. 1-4, Supplementary Tab. 1

Running title
Gamma control of cognitive maturation

One sentence summary
Fast oscillatory activity in layer 2/3 sculpts the maturation of prefrontal cortex and cognitive performance.

Abstract

Gamma oscillations are the neural network attribute of cognitive processing. They emerge early in life, yet their contribution to cortical circuit formation is unknown. We show that layer 2/3 pyramidal neurons entrain mouse prefrontal cortex in fast oscillations with increasing frequency across development. Chronic boosting of fast oscillations at neonatal age reversibly alters neuronal morphology, but cause permanent circuity dysfunction and impairs recognition memory and social interactions later in life.

Main

Synchronization of neuronal activity in fast rhythms is a commonly observed feature in the cerebral cortex [1]. Although its contribution to cognitive performance is still a matter of debate, high frequency oscillatory activity facilitates the communication between neuronal ensembles and is thought to shape information processing in cortical networks [2-4]. Oscillatory activity at frequencies within gamma band has been proposed to emerge from reciprocal interactions of excitatory and inhibitory neurons [1]. Fast inhibitory feedback via soma-targeting parvalbumin (PV)-expressing inhibitory interneurons leads to fast gamma (30-80 Hz) [5,6], whereas dendrite-targeting somatostatin (SST)-expressing inhibitory interneurons contribute to beta/low gamma (20-40 Hz) activity [6,7]. Interneuronal dysfunction and ensuing abnormal gamma activity in the medial prefrontal cortex (mPFC) has been related to impaired cognitive flexibility [8]. Moreover, pyramidal neurons critically contribute to the generation of fast oscillatory rhythms, beyond solely providing the excitatory drive. As recently shown, their feed-forward excitation determines oscillatory dynamics [9].

Despite substantial knowledge linking fast oscillations in the mature cortex and cognitive abilities [8,10,11], their role during development is still largely unknown. Here we examined the emergence of gamma activity in the mouse mPFC across development and assessed the role of fast oscillations for the maturation of prefrontal networks and cognitive abilities. Shifting the level of early oscillatory activity to a transient excessive boosting of fast frequency events, we provide evidence that gamma entrainment of neonatal circuits is critical for the prefrontal function and behavioral performance of adults.

Extracellular recordings in the mPFC of postnatal day (P) 5-40 mice revealed that fast frequency oscillations occur spontaneously in awake and urethane-anesthetized mice starting around P8 (Fig. 1a,b and S1a-d). While anesthesia reduced the oscillatory power during development across a broad range of frequencies (Fig. S1e-g), it did not affect the spectral composition of oscillations [12]. In both states, fast frequency oscillations increased in power and frequency with age, reaching stable values around P25 with an adult-like gamma frequency peak at ~50 Hz (Fig. 1c,d). Using a recently established protocol for optogenetic manipulation in neonatal mice [13,14], we interrogated the neuronal substrate of fast oscillatory activity across development. To this end, we transfected ~25% of pyramidal neurons in layers 2/3 (L2/3) by *in utero* electroporation (IUE) with the light-sensitive channelrhodopsin 2 derivate E123T T159C (ChR2(ET/TC)) and stimulated them with ramp light pulses. This stimulation type activates the network without imposing a specific rhythm, thus enabling neurons to fire at their preferred frequencies. We focused on neurons from L2/3 because our previous investigations identified them as drivers of fast oscillatory rhythms at neonatal age [13]. This layer-specificity seems to be a developmental feature of mPFC, since recent work in adult sensory cortices has shown that gamma rhythms can be driven by pyramidal neurons from all layers [15,16]. We found that light-driven fast oscillatory activity increased in power and frequency across development, similarly to what we observed for spontaneous oscillations (Fig. 1e-k and S1h-l). This increase co-occurred with the maturation of PV-expressing interneurons (Fig. S2a,b) and the maturation of inhibitory synapses on excitatory neurons [17,18]. Therefore, a developmental transition from SST-dominated to PV-dominated feedback inhibition might underlie the gamma frequency increase across development. Alternatively, increased gamma frequency with age might result from

alterations in the biophysical properties underlying excitability and maximal firing rate of cortical pyramidal neurons [19]. Indeed, we found that the firing rate and amplitude of single unit activity (SUA) increased with age, whereas its half width decreased (Fig. S2c-e). To disentangle the role of interneurons from that of pyramidal neurons for the generation of fast oscillations across development, we transfected L2/3 pyramidal neurons with ChR2(ET/TC) by IUE in transgenic mice expressing archaerhodopsin3 (ArchT) in all interneurons. Silencing of interneurons led to a broadband increase of activity in fast frequencies (>12 Hz) that was most pronounced in neonatal mice (Fig. S2f-i). However, silencing of interneurons did not affect gamma activity driven by light stimulation of L2/3 neurons, demonstrating a critical role of pyramidal neurons for the generation of gamma rhythmicity.

The presence of neuronal ensembles capable of generating fast oscillatory rhythms during early development raises the question of whether this pattern of activity solely reflects or directly contributes to the maturation of cortical circuits and their functions. Abundant literature documented the role of coordinated electrical activity for dendrite formation, synaptic pruning and apoptosis [20-22]. To elucidate the role of neonatal fast oscillatory activity for prefrontal network maturation, we established here an optogenetic protocol for chronic early stimulation (ES) of L2/3 pyramidal neurons at the age when fast oscillations start to occur in the mPFC (Fig. 2a) [23]. ES mice were stimulated daily from P7-11 with blue light ramps (473 nm), whereas control animals were similarly stimulated, but with yellow light ramps (594 nm) that do not activate ChR2(ET/TC). Both intra- and transcranial ramp light stimulation acutely boosted network oscillations in beta-low gamma frequency range in neonatal mice (Fig. 2b).

First, we assessed the effects of ES on the morphology of L2/3 pyramidal neurons. Immediately after stimulation, light-induced boosting of fast oscillatory activity led to an exhaustive and premature growth of dendrites of L2/3 pyramidal neurons (Fig. 2c,d). At P11-12, stimulated neurons reached a dendritic length (3166 ± 632 μm) significantly higher than of age-matched controls (2029 ± 244 μm, p=0.007) but comparable to that of control animals at P23-25 (3356 ± 356 μm). These effects were transient, such that the dendritic complexity and length of L2/3 pyramidal neurons was largely unchanged in P23-25 (ES: 2906.5 ± 860.5 μm, p=0.631) and P38-40 (control: 4202 ± 625.5 μm; ES: 3746. 5± 630.5 μm, p=0.162) ES mice. Surprisingly, ES caused a transient reduction of GABA-positive neurons (Fig. 2e). The survival of interneurons has been shown to depend on the level of excitatory input during early postnatal development [20,24]. Therefore, the reduction of interneuron density might be explained by the fact that optogenetic stimulation and subsequent augmented firing of transfected neurons (~25% of total pyramidal neurons) reduces the overall level of activity, due to surround suppression [7,15].

Next, we monitored the ES effects on functional network maturation. Extracellular recordings from the mPFC of P11-12, P23-25 and P38-40 control and ES mice were performed simultaneously with light stimulation of ChR2(ET/TC)-transfected L2/3 pyramidal neurons. Acutely stimulated activity was similar in control and ES mice at P11-12, whereas at P23-25 the induced oscillatory peak slightly decreased, yet not at significant level. At P38-40, the amplitude of driven oscillations in gamma band was significantly reduced in both anesthetized (modulation index, P38-40: control: 0.72 ± 0.16; ES: 0.19 ± 0.24, p=0.025) (Fig. 3a-c) and awake (modulation index, P38-40: control: 0.72 ± 0.06; ES: 0.50 ± 0.17, p=0.043) (Fig. S3f,g) ES mice when compared to

controls. Bilateral recordings from all prefrontal layers in ES mice revealed that interlayer as well as interhemispheric gamma frequency coherence was reduced at P38-40 when compared to controls (Fig. 3d-i). In contrast, spontaneous activity of mPFC did not differ between controls and ES mice across development (Fig. S3a-e), indicating that perturbation of fast neonatal rhythms might solely disrupt the ability of local circuits to respond to activation (i.e. under physiological conditions: stimulus, task). Of note, the reduction of L2/3 driven gamma activity in ES mice occurred towards the end of juvenile development, when dendritic morphology and interneuron number had largely recovered (Fig. 2d,e).

Gamma activity is thought to affect information processing in adult mPFC and, ultimately, behavior [8,10,11]. Weaker gamma entrainment of prefrontal circuits after interfering with fast oscillatory activity through ES at neonatal age might come along with compromised cognitive abilities. We used a battery of tests to examine mPFC-dependent behavior of ES and control mice at P16-36. To avoid confounding effects, we ascertained that ES mice have normal somatic and reflex development (Fig. S4a). Their open field behavior was also normal (Fig. S4b). However, ES mice failed to distinguish between objects in mPFC-dependent novel object and recency recognition tasks, but not in a hippocampus-dependent object location recognition task (Fig. 4a,b and S4c). Moreover, they showed abnormal social interactions as mirrored by reduced interaction time with the mother (Fig. 4c). Spatial working memory was also impaired as revealed by significant deficits of ES mice in 8-arm maze test (Fig. 4d). In contrast, spatial alteration and tail suspension were not affected (Fig. S4d,e). Combined analysis of behavioral performance throughout the different tests with support vector classification and 5-fold cross-validation yielded a correct classification of control and ES mice in 77%

in the training and 78% in the test data set (Fig. 4e). Thus, the cognitive deficits at adulthood are reliable markers of functional imbalance within neonatal prefrontal circuitry.

Gamma oscillations are highly relevant for adult cortical function [3,4,25] and dysfunction [8,26], yet their development is still poorly understood. The results of the present study (i) provide insights into the age-dependent mechanisms of early fast oscillations and (ii) demonstrate their relevance for the functional maturation of prefrontal networks as well as cognitive and social abilities. Throughout development, L2/3 pyramidal neurons have been identified as key players for the generation of fast oscillations in the mPFC. Their activation led to activity patterns with similar features as spontaneously-generated gamma oscillations. With age, the fast rhythms become more prominent. The frequency and amplitude increase results from the maturation of electrical properties of pyramidal neurons but also from the progressive embedding of PV-expressing fast-spiking interneurons into circuits initially controlled by SST-expressing interneurons [27,28].

Do fast oscillations during development simply mirror neural maturation or do they contribute to circuit refinement? This key question has been previously approached for sensory systems with defined cortical topography. Neonatal fast oscillations have been proposed to facilitate the formation of topographic units through input replay in somatosensory thalamocortical circuits [29]. In visual cortex, gamma activity depends on visual experience and has been proposed as an indicator of cortical maturity [30]. Being not directly driven by corresponding environmental stimuli or sensory periphery, limbic circuits follow distinct developmental rules. Emergence of oscillation-coupled prefrontal ensembles at a developmental stage when the mice are blind, deaf and lack whisking

and motor abilities, is driven by hippocampal theta oscillations [23,31]. They result, on their turn, from activation of lateral entorhinal cortex under the control of olfactory stimuli [32,33]. Excitatory hippocampal projections targeting L5/6 neurons promote interlaminar interactions within mPFC centered on coordinated activation of L2/3 pyramidal neurons. Boosting this neonatal process through chronic light stimulation of L2/3 pyramidal neurons seems to push the system out of an optimum level of activity and synchrony. The direct consequences are transient structural changes (exuberant dendritic arborization, decreased density of interneurons) that are compensated before adulthood. However, the function of prefrontal circuits appears permanently compromised after ES. The weaker gamma entrainment of adult prefrontal circuits contributes to poorer performance in behavioral tasks that require mPFC, such as novel and recency recognition, working memory as well as social interaction. These results uncover the role of neonatal oscillations for the maturation of limbic circuit function and cognitive abilities.

The mechanisms described here might explain cognitive difficulties of preterm born humans that experience excessive sensory stimulation in neonatal intensive care unit (NICU) at a comparable stage of brain development (2nd-3rd gestational trimester) [34,35]. These stressful stimuli might trigger premature gamma entrainment, perturbing the activity-dependent maturation of cortical networks (Moiseev et al., 2015). Frontal regions have been reported to be particularly vulnerable to NICU conditions [36] and correspondingly, preterm children highly prone to frontally-confined impairment, such as memory and attention deficits (Taylor and Clark, 2016). Thus, our findings lend support to the concept that fast network oscillations have a central role for neurodevelopmental disorders [37,38].

References

1 Buzsaki, G. *Rhythms of the Brain*. (Oxford University Press, 2006).

2 Singer, W. Neuronal oscillations: unavoidable and useful? *Eur J Neurosci* **48**, 2389-2398.

3 Cardin, J. A. Snapshots of the Brain in Action: Local Circuit Operations through the Lens of gamma Oscillations. *Journal of Neuroscience* **36**, 10496-10504.

4 Sohal, V. S. How Close Are We to Understanding What (if Anything) gamma Oscillations Do in Cortical Circuits? *Journal of Neuroscience* **36**, 10489-10495.

5 Cardin, J. A. *et al.* Driving fast-spiking cells induces gamma rhythm and controls sensory responses. *Nature* **459**, 663-667.

6 Chen, G. *et al.* Distinct Inhibitory Circuits Orchestrate Cortical beta and gamma Band Oscillations. *Neuron* **96**, 1403-1418 e1406.

7 Veit, J., Hakim, R., Jadi, M. P., Sejnowski, T. J. & Adesnik, H. Cortical gamma band synchronization through somatostatin interneurons. *Nat Neurosci* **20**, 951-959.

8 Cho, K. K. *et al.* Gamma rhythms link prefrontal interneuron dysfunction with cognitive inflexibility in Dlx5/6(+/-) mice. *Neuron* **85**, 1332-1343.

9 Nicholson, E., Kuzmin, D. A., Leite, M., Akam, T. E. & Kullmann, D. M. Analogue closed-loop optogenetic modulation of hippocampal pyramidal cells dissociates gamma frequency and amplitude. *Elife* **7**.

10 Cao, W. *et al.* Gamma Oscillation Dysfunction in mPFC Leads to Social Deficits in Neuroligin 3 R451C Knockin Mice. *Neuron* **97**, 1253-1260 e1257.

11 Bastos, A. M., Loonis, R., Kornblith, S., Lundqvist, M. & Miller, E. K. Laminar recordings in frontal cortex suggest distinct layers for maintenance and control of working memory. *Proc Natl Acad Sci U S A* **115**, 1117-1122.

12 Chini, M. G., S.; Kostka, J.K.; Poepplau, J.A.; Cornelissen, L.; Berde, C.B.; Hanganu-Opatz, I.L.; Bitzenhofer S.H. Identifying neurophysiological features associated with anesthetic state in newborn mice and humans. *bioRxiv*.

13 Bitzenhofer, S. H. *et al.* Layer-specific optogenetic activation of pyramidal neurons causes beta-gamma entrainment of neonatal networks. *Nat Commun* **8**, 14563.

14 Bitzenhofer, S. H., Ahlbeck, J. & Hanganu-Opatz, I. L. Methodological Approach for Optogenetic Manipulation of Neonatal Neuronal Networks. *Front Cell Neurosci* **11**, 239.

15 Adesnik, H. & Scanziani, M. Lateral competition for cortical space by layer-specific horizontal circuits. *Nature* **464**, 1155-1160.

16 Adesnik, H. Layer-specific excitation/inhibition balances during neuronal synchronization in the visual cortex. *J Physiol* **596**, 1639-1657.

17 Virtanen, M. A. *et al.* Development of inhibitory synaptic inputs on layer 2/3 pyramidal neurons in the rat medial prefrontal cortex. *Brain Struct Funct* **223**, 1999-2012.

18 Guan, W. *et al.* Eye opening differentially modulates inhibitory synaptic transmission in the developing visual cortex. *Elife* **6**.

19 Oswald, A. M. & Reyes, A. D. Maturation of intrinsic and synaptic properties of layer 2/3 pyramidal neurons in mouse auditory cortex. *J Neurophysiol* **99**, 2998-3008.

20 Wong, F. K. *et al.* Pyramidal cell regulation of interneuron survival sculpts cortical networks. *Nature* **557**, 668-673.

21 Riccomagno, M. M. & Kolodkin, A. L. Sculpting neural circuits by axon and dendrite pruning. *Annu Rev Cell Dev Biol* **31**, 779-805.

22 Anastasiades, P. G. & Butt, S. J. A role for silent synapses in the development of the pathway from layer 2/3 to 5 pyramidal cells in the neocortex. *J Neurosci* **32**, 13085-13099.

23 Brockmann, M. D., Poschel, B., Cichon, N. & Hanganu-Opatz, I. L. Coupled oscillations mediate directed interactions between prefrontal cortex and hippocampus of the neonatal rat. *Neuron* **71**, 332-347.

24 Denaxa, M. *et al.* Modulation of Apoptosis Controls Inhibitory Interneuron Number in the Cortex. *Cell Rep* **22**, 1710-1721.

25 Kim, H., Ahrlund-Richter, S., Wang, X. M., Deisseroth, K. & Carlen, M. Prefrontal Parvalbumin Neurons in Control of Attention. *Cell* **164**, 208-218.

26 Uhlhaas, P. J. & Singer, W. Abnormal neural oscillations and synchrony in schizophrenia. *Nat Rev Neurosci* **11**, 100-113.

27 Tuncdemir, S. N. *et al.* Early Somatostatin Interneuron Connectivity Mediates the Maturation of Deep Layer Cortical Circuits. *Neuron* **89**, 521-535.

28 Mayer, C. *et al.* Developmental diversification of cortical inhibitory interneurons. *Nature* **555**, 457-462.

29 Minlebaev, M., Colonnese, M., Tsintsadze, T., Sirota, A. & Khazipov, R. Early gamma oscillations synchronize developing thalamus and cortex. *Science* **334**, 226-229.

30 Chen, G., Rasch, M. J., Wang, R. & Zhang, X. H. Experience-dependent emergence of beta and gamma band oscillations in the primary visual cortex during the critical period. *Sci Rep* **5**.

31 Ahlbeck, J., Song, L., Chini, M., Bitzenhofer, S. H. & Hanganu-Opatz, I. L. Glutamatergic drive along the septo-temporal axis of hippocampus boosts prelimbic oscillations in the neonatal mouse. *Elife* **7**.

32 Hartung, H., Brockmann, M. D., Poschel, B., De Feo, V. & Hanganu-Opatz, I. L. Thalamic and Entorhinal Network Activity Differently Modulates the Functional Development of Prefrontal-Hippocampal Interactions. *J Neurosci* **36**, 3676-3690.

33 Gretenkord, S. *et al.* Coordinated electrical activity in the olfactory bulb gates the oscillatory entrainment of entorhinal networks in neonatal mice. *PLoS Biol* **17**, e2006994.

34 Moiseev, A., Doesburg, S. M., Herdman, A. T., Ribary, U. & Grunau, R. E. Altered Network Oscillations and Functional Connectivity Dynamics in Children Born Very Preterm. *Brain Topogr* **28**, 726-745.

35 Altimier, L. & Phillips, R. The Neonatal Integrative Developmental Care Model: Advanced Clinical Applications of the Seven Core Measures for Neuroprotective Family-centered Developmental Care. *Newborn and Infant Nursing Reviews* **16**, 230-244.

36 Als, H. *et al.* Early experience alters brain function and structure. *Pediatrics* **113**, 846-857.

37 Peiker, I. *et al.* Perceptual Integration Deficits in Autism Spectrum Disorders Are Associated with Reduced Interhemispheric Gamma-Band Coherence. *Journal of Neuroscience* **35**, 16352-16361.

38 Chini, M. L., C.; Poepplau, J. A.; Xu, X.; Ahlbeck, J.; Bitzenhofer, S. H.; Mulert, C.; Hanganu-Opatz, I. L. Microglia inhibition rescues developmental hypofrontality in a mouse model of mental illness. *bioRxiv*.

Acknowledgments

We thank P. Putthoff, A. Dahlmann, and K. Titze for excellent technical assistance. This work was funded by grants from the European Research Council (ERC-2015-CoG 681577 to I.L.H.-O.) and the German Research Foundation (Ha 4466/10-1, Ha4466/11-1, Ha4466/12-1, SPP 1665, SFB 936 B5 to I.L.H.-O.).

I.L. H.-O. is founding member of FENS Kavli Network of Excellence.

Author contributions: S.H.B. and I.L.H.-O. designed the experiments, S.H.B., J.A.P and A.M. carried out the experiments, S.H.B., J.A.P. and M.C. analyzed the data, S.H.B., I.L.H.-O., M.C and J.A.P interpreted the data and wrote the manuscript. All authors discussed and commented on the manuscript.

Figures

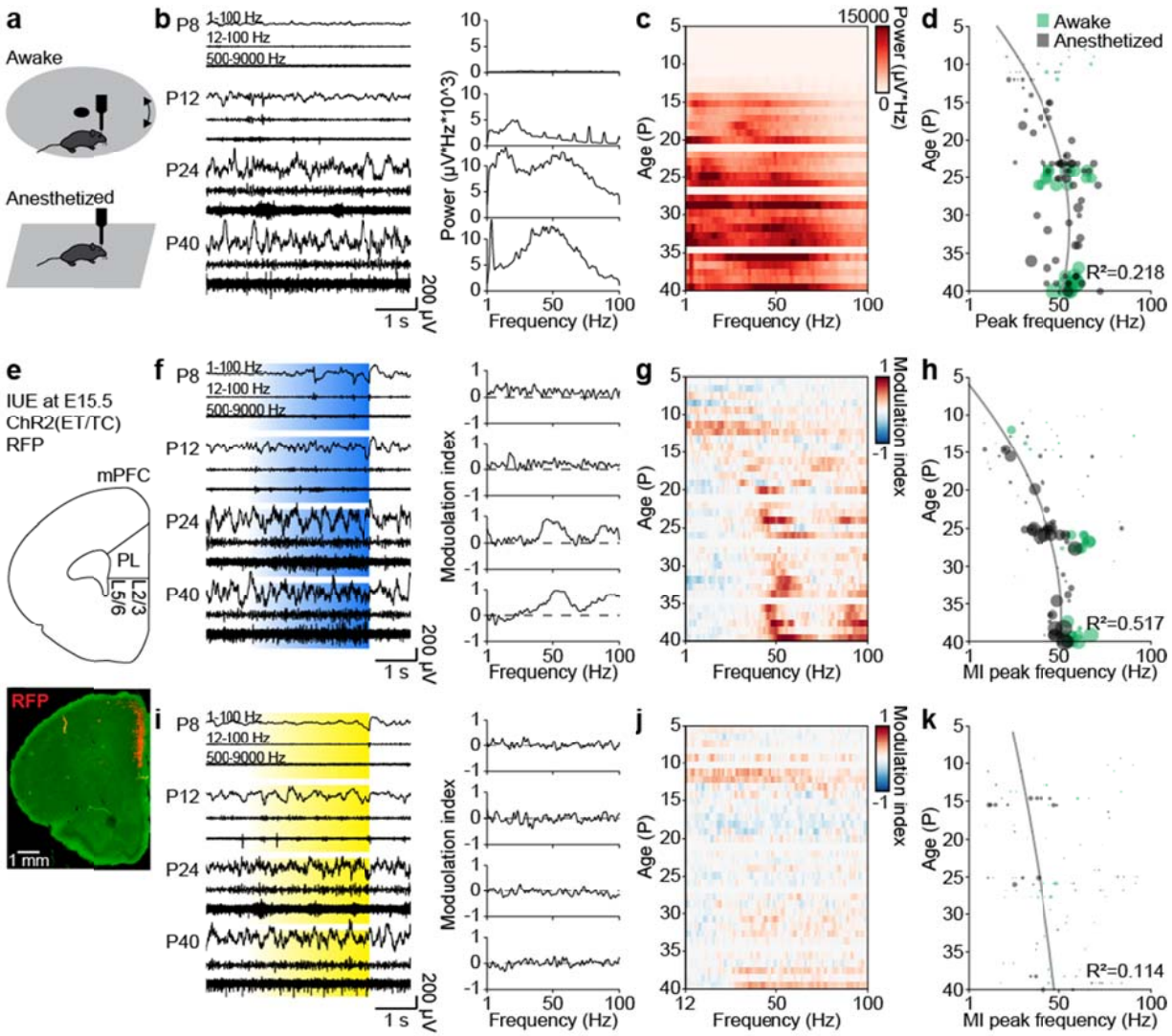

Fig. 1. Age dependence of fast rhythmic activity in the developing mPFC. (**a**) Schematic of the recording paradigms in awake (head-fixed on a movable disk) and anesthetized (head-fixed) P5-40 mice. (**b**) Example local field potentials (LFPs) from mPFC of awake mice at different ages after band-pass filtering (left) accompanied by the corresponding power spectra (right). (**c**) Color-coded power spectra of spontaneous oscillatory activity averaged over each age for P5-40 mice (n=80). (**d**) Scatter plot displaying the age-dependence of peak frequencies of fast oscillations (12-100 Hz) for anesthetized (n=80) and awake mice (n=20, 35 recordings). Marker size displays peak strength. (**e**) ChR2(ET/TC)-2A-RFP-expression in L2/3 pyramidal neurons in mPFC after IUE at E15.5 in a coronal slice of a P10 mouse. (**f**) Example LFPs driven by ramp light

stimulations (473 nm, 3 s) of L2/3 pyramidal neurons in mPFC at different ages (left) accompanied by the corresponding modulation index (MI) of power spectra normalized to pre-stimulus (right). (**g**) Color-coded normalized (during-to-before stimulation) MI of power spectra averaged over age for P5-40 mice (n=80). (**h**) Scatter plot displaying the age-dependence of stimulus induced peak frequencies across development for anesthetized (n=80) and awake mice (n=20, 35 recordings). Marker size displays peak strength. (**i-k**) Same as F-H for control ramp light stimulations (594 nm, 3s). See Supplementary Tab. 1 for detailed information on statistics. Average data is presented as median ± MAD.

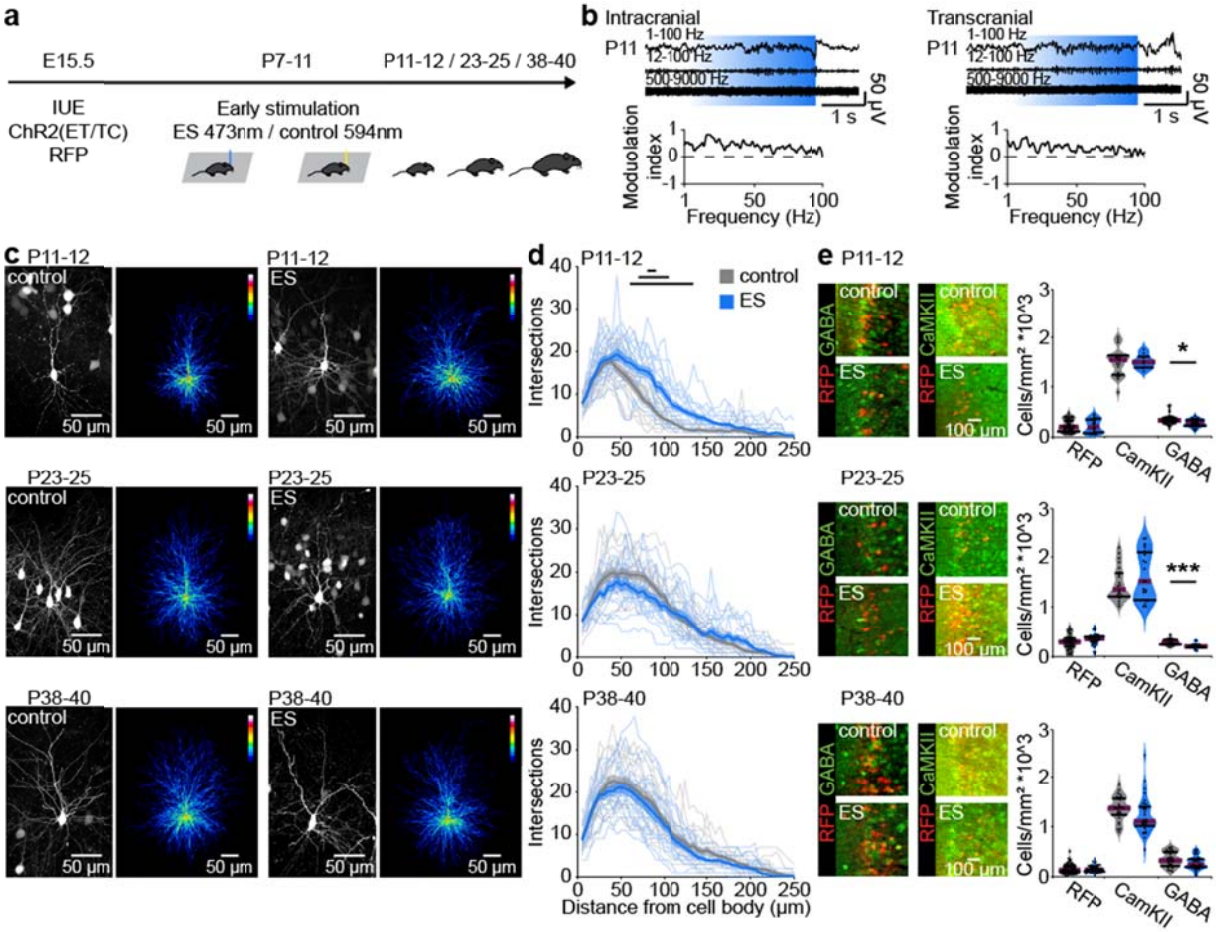

Fig. 2. Structural alterations in mPFC as result of ES of L2/3 pyramidal neurons in mPFC. (**a**) Schematic timeline of manipulations as well as morphological, functional, and behavioral assessment. (**b**) Example of LFPs driven by intracranial (left) and transcranial (right) ramp light stimulations of L2/3 pyramidal neurons in mPFC (top) displayed together with the corresponding MI of power spectra (bottom) for a P11 mouse. (**c**) Example pictures and average heat maps of IUE-transfected L2/3 pyramidal neurons for control (left) and ES mice (right) at P11-12, P23-25 and P38-40. (**d**) Line plots of dendritic intersections averaged for L2/3 pyramidal neurons within a 250 µm radius from the soma center for control and ES mice at P11-12 (condition p=2.2e-16), P23-25 (condition p=2.2e-16) and P38-40 (condition p=2.4e-5) (control, 18 cells of 3 mice / age group; ES 18 cells of 3 mice / age group). Thin lines correspond to individual neurons. (**e**) Left, GABA and CaMKII immunostainings of prefrontal neurons from control and ES mice at P11-12, P23-25 and P38-40. Right, violin plots of RFP-transfected, CaMKII-positive and GABA-positive neuron density in prefrontal L2/3 of control and ES mice

(right). *P<0.05, **P<0.01 and ***P<0.001. See Supplementary Tab. 1 for detailed information on statistics. Average data is presented as median ± MAD.

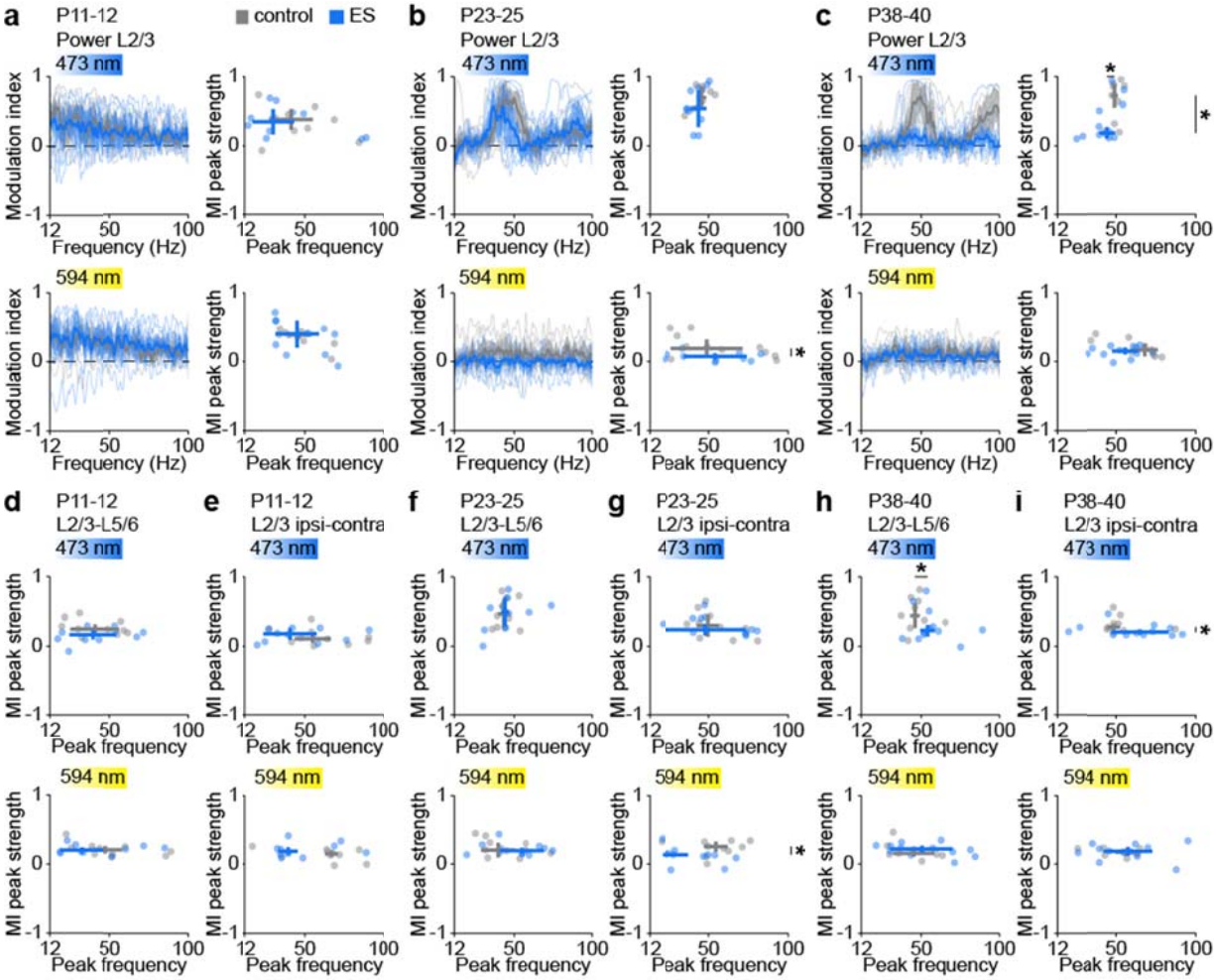

Fig. 3. Prefrontal dysfunction as result of ES of L2/3 pyramidal neurons in mPFC. (**a**) Top left, MI of power spectra of light-driven activity (ramp, 473 nm, 3s) for control and ES mice at P11-12 (control n=10, ES n=10). Top right, scatter plot displaying corresponding MI power peak strength as a function of peak frequency. Bottom left and right, same as top for control stimulation (ramp, 594 nm, 3s). (**b**) Same as (a) for P23-25 mice (control n=10, ES n=11). (**c**) Same as (a) for P38-40 mice (control n=9, ES n=12). (**d**) Scatter plots displaying the peak strength as a function of peak frequency for the MI of imaginary coherence between light-driven L2/3 and ipsilateral L5/6 in the mPFC of control and ES mice for stimulation (473 nm) and control stimulation (594 nm). (**e**) Scatter plots displaying the peak strength as a function of peak frequency for the MI of imaginary coherence between light-driven L2/3 and contralateral L2/3 in the mPFC of control and ES mice for stimulation (473 nm) and control stimulation (594 nm). (**f,g**) Same as (d,e) for P23-25 mice. (**h,i**) Same as (d,e) for P38-40 mice. *P<0.05, **P<0.01

and ***P<0.001. See Supplementary Tab. 1 for detailed information on statistics. Average data is presented as median ± MAD.

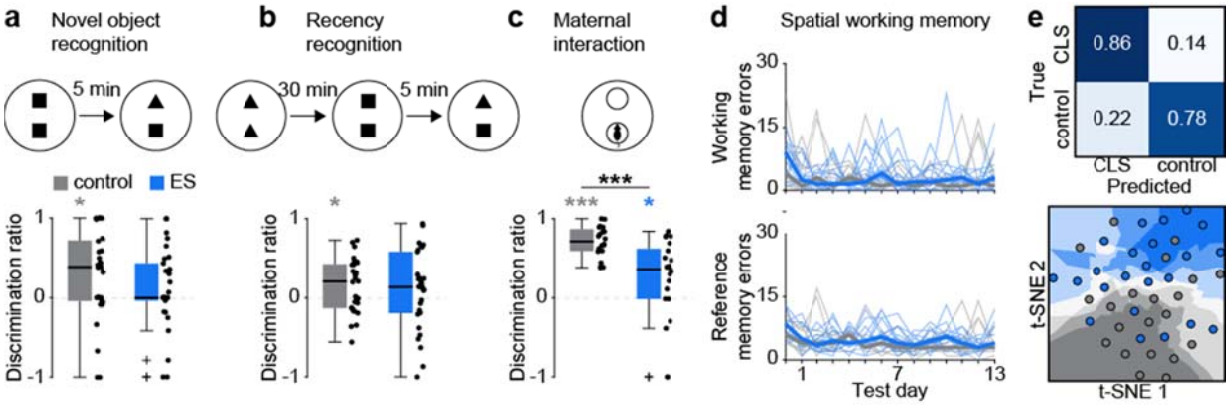

Fig. 4. Poorer cognitive and social performance of mice experiencing ES of L2/3 pyramidal neurons in mPFC. (**a**) Top, schematic of novel object recognition task. Bottom, discrimination ratio of interaction time with a novel-to-familiar object for P17 control (n=28) and ES mice (n=30). (**b**) Top, schematic of recency recognition task. Bottom, discrimination ratio of interaction time with a less-to-more recent object for P22 control (n=28) and ES mice (n=30). (**c**) Top, schematic of maternal interaction task. Bottom, discrimination ratio of interaction time with a mother-to-empty bin for P21 control (n=19) and ES mice (n=21). (**d**) Spatial working (condition p=0.007) and reference memory (condition p=0.001) performance for P23-36 control (n=10) and ES mice (n=12) in an 8-arm radial maze with 4 baited arms over 14 consecutive days. (**e**) Confusion matrix (top) and decision space (bottom) as well as single data points for support vector machine classification used to predict if an animal belongs to control or ES based on combined behavioral performance. Fill color of single data points represents true condition. *P<0.05, **P<0.01 and ***P<0.001. See Supplementary Tab. 1 for detailed information on statistics. Average data is presented as median ± MAD.

List of supplementary materials

Methods

Fig. S1 (related to Fig. 1): Spontaneous and L2/3-driven activity in awake and anesthetized mice across development

Fig. S2 (related to Fig. 1): Neurochemical profile and firing patterns in PFC across development.

Fig. S3 (related to Fig. 3): ES effects on spontaneous and L2/3 pyramidal neuron-driven activity in anesthetized and awake head-fixed mice across development

Fig. S4 (related to Fig. 4): Developmental milestones and behavioral performance after ES of L2/3 pyramidal neurons in the mPFC

Supplementary Tab. 1: Statistics summary

Supplementary materials for:

Activity-dependent maturation of prefrontal gamma oscillations sculpts cognitive performance

Sebastian H. Bitzenhofer[1,*], Jastyn A. Pöpplau[1], Mattia Chini[1], Annette Marquardt[1], Ileana L. Hanganu-Opatz[1,*]

[1] Developmental Neurophysiology, Institute of Neuroanatomy, University Medical Center Hamburg-Eppendorf, Hamburg, Germany

* Corresponding authors: Ileana L. Hanganu-Opatz
hangop@zmnh.uni-hamburg.de
Falkenried 94, 20251 Hamburg, Germany

Sebastian H. Bitzenhofer
sebastian.bitzenhofer@zmnh.uni-hamburg.de
Falkenried 94, 20251 Hamburg, Germany

List of supplementary materials

Methods

Supplementary Fig.1 (related to Fig. 1): Spontaneous and L2/3-driven activity in awake and anesthetized mice across development

Supplementary Fig.2 (related to Fig. 1): Neurochemical identity and firing patterns in PFC across development.

Supplementary Fig.3 (related to Fig. 3): ES effects on spontaneous and L2/3 pyramidal neuron-driven activity in anesthetized and awake head-fixed mice across development

Supplementary Fig.4 (related to Fig. 4): Developmental milestones and behavioral performance after ES of L2/3 pyramidal neurons in the mPFC

Supplementary Tab. 1: Statistics summary

Methods

Animals

All experiments were performed in compliance with the German laws and the guidelines of the European Community for the use of animals in research and were approved by the local ethical committee (G132/12, G17/015, N18/015). Experiments were carried out on C57Bl/6J mice of both sexes. To achieve interneuron-specific expression of archaerhodopsin-3 (ArchT), Gad2 driver line (Gad2-IRES-Cre knock-in, The Jackson Laboratory, ME, USA) was crossed with Ai40 reporter line (Ai40(RCL-ArchT/EGFP)-D, The Jackson Laboratory, ME, USA). Timed-pregnant mice from the animal facility of the University Medical Center Hamburg-Eppendorf were housed individually at a 12 h light/12 h dark cycle and were given access to water and food ad libitum. The day of vaginal plug detection was considered E0.5, the day of birth was considered P0.

In utero electroporation

Pregnant mice received additional wet food on a daily basis, supplemented with 2-4 drops Metacam (0.5 mg/ml, Boehringer-Ingelheim, Germany) one day before until two days after *in utero* electroporation. At E15.5, pregnant mice were injected subcutaneously with buprenorphine (0.05 mg/kg body weight) 30 min before surgery. Surgery was performed under isoflurane anesthesia (induction 5%, maintenance 3.5%) on a heating blanket. Eyes were covered with eye ointment and pain reflexes and breathing were monitored to assess anesthesia depth. Uterine horns were exposed and moistened with warm sterile PBS. 0.75-1.25 µl of opsin- and fluorophore-encoding plasmid (pAAV-CAG-ChR2(E123T/T159C)-2A-tDimer2, 1.25 µg/µl) purified with NucleoBond (Macherey-Nagel, Germany) in sterile PBS with 0.1% fast green dye was injected in the right lateral ventricle of each embryo using pulled borosilicate glass

capillaries. Electroporation tweezer paddles of 5 mm diameter were oriented at a rough 20° leftward angle from the midline of the head and a rough 10° downward angle from the anterior to posterior axis to transfect precursor cells of medial prefrontal L2/3 pyramidal neurons with 5 electroporation pulses (35 V, 50 ms, 950 ms interval, CU21EX, BEX, Japan). Uterine horns were placed back into the abdominal cavity. Abdominal cavity was filled with warm sterile PBS and abdominal muscles and skin were sutured with absorbable and non-absorbable suture thread, respectively. After recovery from anesthesia, mice were returned to their home cage, placed half on a heating blanket for two days after surgery. Fluorophore expression was assessed at P2 in the pups with a portable fluorescence flashlight (Nightsea, MA, USA) through the intact skin and skull and confirmed in brain slices post mortem.

Early stimulation (ES)

A stimulation window was implanted at P7 for chronic transcranial optogenetic stimulation in mice transfected by *in utero* electroporation. Mice were placed on a heating blanket and anesthetized with isoflurane (5% induction, 2% maintenance). Breathing and pain reflexes were monitored to assess anesthesia depth. The skin above the skull was cut along the midline (3 mm) at the level of the mPFC and gently spread with a forceps, before covering the incision with transparent tissue adhesive (Surgibond, SMI, Belgium). Mice were returned to the dam in the home cage after recovery from anesthesia. From P7-11 mice were stimulated daily under isoflurane anesthesia (5% induction, 2% maintenance) with ramp stimulations of linearly increasing light power (473 nm wavelength, 3 s duration, 7 s interval, 180 repetitions, 30 min total duration). Light stimulation was performed using an Arduino uno (Arduino, Italy) controlled laser system (Omicron, Austria) coupled to a 200 µm diameter light fiber (Thorlabs, NJ, USA)

positioned directly above the tissue adhesive window. Light power attenuation was set to reach 10 mW in the brain, adjusted for measured light attenuation by the tissue adhesive (~30%) and by the immature skull (~25%). Control animals were treated identical, but stimulated with light of 594 nm wavelength that does not activate the expressed opsin ChR2(ET/TC).

Optogenetics and electrophysiology in vivo

Acute recordings. Multi-site extracellular recordings of local field potential (LFP) and multi-unit activity (MUA) were performed unilaterally or bilaterally in the mPFC of non-anesthetized or anesthetized P5-40 mice. Pups were on a heating blanket during the entire procedure. Under isoflurane anesthesia (induction: 5%; maintenance: 2.5%), a craniotomy was performed above the mPFC (0.5 mm anterior to bregma, 0.1-0.5 mm lateral to the midline). Neck muscles were cut and 0.5% bupivacaine / 1% lidocaine was locally applied to cutting edges. Pups were head-fixed into a stereotaxic apparatus using two plastic bars mounted on the nasal and occipital bones with dental cement. Multi-site electrodes (NeuroNexus, MI, USA) were inserted into the mPFC (four-shank, A4x4 recording sites, 100 µm spacing, 125 µm shank distance, 1.8-2.0 mm deep). A silver wire was inserted into the cerebellum and served as ground and reference. Pups were allowed to recover for 30 min prior to recordings. For anesthetized recordings, urethane (1 mg/g body weight) was injected intraperitoneally prior to the surgery. Extracellular signals were band-pass filtered (0.1-9,000 Hz) and digitized (32 kHz) with a multichannel extracellular amplifier (Digital Lynx SX; Neuralynx, Bozeman, MO, USA). Electrode position was confirmed in brain slices post mortem.

Chronic recordings. Multisite extracellular recordings were performed in the mPFC of P23-25 and P38-40 mice. The adapter for head fixation was implanted at least 5 days

before recordings. Under isoflurane anesthesia (5% induction, 2.5% maintenance), a metal head-post (Luigs and Neumann, Germany) was attached to the skull with dental cement and a craniotomy was performed above the mPFC (0.5-2.0 mm anterior to bregma, 0.1-0.5 mm right to the midline) and protected by a customized synthetic window. A silver wire was implanted between skull and brain tissue above the cerebellum and served as ground and reference. 0.5% bupivacaine / 1% lidocaine was locally applied to cutting edges. After recovery from anesthesia, mice were returned to their home cage. After recovery from the surgery, mice were accustomed to head-fixation and trained to run on a custom-made spinning disc. For recordings, craniotomies were uncovered and multi-site electrodes (NeuroNexus, MI, USA) were inserted into the mPFC (one-shank, A1x16 recording sites, 100 µm spacing, 2.0 mm deep). Extracellular signals were band-pass filtered (0.1-9000 Hz) and digitized (32 kHz) with a multichannel extracellular amplifier (Digital Lynx SX; Neuralynx, Bozeman, MO, USA). Electrode position was confirmed in brain slices post mortem.

Optogenetic stimulation. Pulsed (light on-off) and ramp (linearly increasing light power) light stimulation was performed using an Arduino uno (Arduino, Italy) controlled laser system (473 nm / 594 nm wavelength, Omicron, Austria) coupled to a 50 µm (4 shank electrodes) or 105 µm (1 shank electrodes) diameter light fiber (Thorlabs, NJ, USA) glued to the multisite electrodes, ending 200 µm above the top recording site.

Histology

P5-40 mice were anesthetized with 10% ketamine (aniMedica, Germanry) / 2% xylazine (WDT, Germany) in 0.9% NaCl (10 µg/g body weight, intraperitoneal) and transcardially perfused with 4% paraformaldehyde (Histofix, Carl Roth, Germany). Brains were removed and postfixed in 4% paraformaldehyde for 24 h. Brains were sectioned

coronally with a vibratom at 50 µm for immunohistochemistry or 100 µm for examination of dendritic complexity.

Immunohistochemistry. Free-floating slices were permeabilized and blocked with PBS containing 0.8% Triton X-100 (Sigma-Aldrich, MO, USA), 5% normal bovine serum (Jackson Immuno Research, PA, USA) and 0.05% sodium azide. Slices were incubated over night with primary antibody rabbit-anti-GABA (1:1000, #A2052, Sigma-Aldrich, MMO, USA), rabbit-anti-Ca2+/calmodulin-dependent protein kinase II (1:200, #PA5-38239, Thermo Fisher, MA, USA; 1:500, #ab52476, Abcam, UK), rabbit-anti-parvalbumin (1:500, #ab11427, Abcam, UK) or rabbit-anti-somatostatin (1:250, #sc13099, Santa Cruz, CA, USA), followed by 2 h incubation with secondary antibody goat-anti-rabbit Alexa Fluor 488 (1:500, #A11008, Invitrogen-Thermo Fisher, MA, USA) or goat-anti-rat Alexa Fluor 488 (1:750, #A11006, Invitrogen-Thermo Fisher, MA, USA). Sections were transferred to glass slides and covered with Fluoromount (Sigma-Aldrich, MO, USA).

Cell quantification. Images of immunofluorescence in the right mPFC as well as IUE-induced tDimer2 expression were acquired with a confocal microscope (DM IRBE, Leica, Germany) using a 10x objective (numerical aperture 0.3). tDimer2-positive and immunopositive cells were automatically quantified with custom-written algorithms in ImageJ environment. The region of interest (ROI) was manually defined over L2/3 of the mPFC. Image contrast was enhanced before applying a median filter. Local background was subtracted to reduce background noise and images were binarized and segmented using the watershed function. Counting was done after detecting the neurons with the extended maxima function of the MorphoLibJ plugin.

Dendritic complexity. Image stacks of tDimer2-positive neurons were acquired with a confocal microscope (LSN700, Zeiss, Germany) using a 40x objective. Stacks of 6 neurons per animal were acquired as 2048x2048 pixel images (voxel size 156*156*500 nm). Dendritic complexity was quantified by Sholl analysis in ImageJ environment. Images were binarized using auto threshold function and the dendrites were traced using the semi-automatic simple neurite tracer plugin. The geometric center was identified and the traced dendritic tree was analyzed with the Sholl analysis plugin.

Behavior

Mice were handled and adapted to the room of investigation daily starting two days prior to behavioral examination. Arenas and objects were cleaned with 0.1% acetic acid before each trial. Animals were tracked automatically (Video Mot2, TSE Systems GmbH, Germany).

Developmental milestones. Somatic and reflex development was examined from P2-20 at a 3-day interval. Weight, body length and tail length were measured. Grasping reflex was assessed by touching front paws with a toothpick. Vibrissa placing was measured as head movement in response to gently touching the vibrissa with a toothpick. Auditory startle was assessed in response to finger snapping. The days of pinnae detachment and eye opening were monitored. Surface righting was measured as time to turn around after being positioned on the back (max 30 s). Cliff avoidance was measured as time until withdrawing after being positioned with forepaws and snout over an elevated edge (max 30 s). Bar holding was measured as time hanging on an toothpick grasped with the forepaws (max 10 s).

Open field. Each mouse was positioned in the center of a circular arena individually (34 cm in diameter) at P16 for 10 min. Behavior was quantified by measuring: discrimination

index of time spent in the center and the border of the arena ((time in surround - time in center) / (time in surround + time in center)), grooming time, average velocity and number of rearing, wall rearing and jumping.

Object recognition. Novel object recognition (NOR, P17), object location recognition (OLR, P18) and recency recognition (RR, P21) were performed in the same arena as the open field examination. Mouse center, tail and snout position were tracked automatically. Object interaction was defined as the snout being within <1 cm distance from an object. For NOR, each mouse explored two identical objects for 10 min during the sample phase. After a delay period of 5 min in a break box, the mouse was placed back in the arena for the test phase where one of the objects was replaced by a novel object. Behavior was quantified as discrimination index of time spent interacting with the novel and familiar object ((time novel object - time familiar object) / (time novel object + time familiar object)). OLR was performed similarly, but one object was relocated for the test phase instead of being exchanged. For RR, each mouse explored two identical objects during the first sample phase for 10 min, followed by a delay phase of 30 min, and a second sample phase of 10 min with two novel identical objects. After a second break of 5 min, time interacting with an object of the first sample phase (old) and an object from the second sample phase (recent) was assessed during the test phase for 2 min. Behavior was quantified as discrimination index of time spent interacting with the novel and familiar object ((time old object – time recent object) / (time old object + time recent object)).

Maternal interaction. Maternal interaction was performed at P21 in the same arena as the open field examination with two plastic containers, one empty and one containing the dam of the mouse pup examined. Small holes in the containers allowed the pup and the

mother to interact. Behavior was quantified as discrimination index of time spent interacting with the empty container and the container containing the mother ((time mother container – time empty container) / (time mother container + time empty container)).

Spontaneous alteration. At P15, 18 and 21, each mouse was positioned on the central arm of an elevated t-maze. After 1 min, the mouse had access to one of the other arms. The mouse was placed back in the start arm for 1 min, before a second run. Behavior was quantified as alteration or no alteration between the two arms in the first and second run.

Tail suspension. Mice were fixed with their tail on a bar 30 cm above ground for 5 min at P21. Behavior was quantified as time spent inactive, passively hanging.

Spatial working memory. Mice were positioned in the center of an elevated 8-arm radial maze daily from P23-36. Arms were without walls and 4 arms contained a food pellet at the distal end (baited). On the first day, mice were allowed to examine the maze for 20 min or until all arms were visited. During the following days, mice were allowed to examine the maze until all baited arms were visited, but for max 20 min and arm entries were assessed. Visit of a non-baited arm was considered as reference memory error, repeated visit of the same arm in one trial as working memory error.

Data analysis

In vivo data were analyzed with custom-written algorithms in Matlab environment. Data were band-pass filtered (500-9000 Hz for spike analysis or 1-100 Hz for LFP) using a third-order Butterworth filter forward and backward to preserve phase information before down-sampling to analyze LFP.

Power spectral density. For power spectral density analysis, 2 s-long windows of LFP signal were concatenated and the power was calculated using Welch's method with non-overlapping windows. Spectra were multiplied with squared frequency.

Imaginary coherence. The imaginary part of complex coherence, which is insensitive to volume conduction, was calculated by taking the absolute value of the imaginary component of the normalized cross-spectrum.

Modulation index. For optogenetic stimulations, modulation index was calculated as (value stimulation - value pre stimulation) / (value stimulation + value pre stimulation).

Peak frequency and strength. Peak frequency and peak strength were calculated for the most prominent peak in the spectrum defined by the product of peak amplitude, peak half width and peak prominence.

Single unit analysis. Spikes were detected and sorted with Ultra Mega Sort 2000 software in Matlab.

Support vector classification. Model training and performance evaluation were carried out using the scikit-learn toolbox in Python. The set was iteratively (n=500) divided using 5-fold cross-validation in a training (4/5) and a test (1/5) set. The value of the model regularization parameter "C" was tuned on the training set, which was further split using 3-fold cross-validation. Model prediction was assessed on the test set. Performance was stable across a wide range of regularization parameter values. To plot the classifier decision space, we used t-sne to reduce the feature space to two dimensions, while preserving the hyper-dimensional structure of the data. The decision space was then approximated by imposing a Voronoi tessellation on the 2d plot, using k-nearest regression on the t-sne coordinates of the predicted classes of the mice.

Statistics. Statistical analyses were performed in the Matlab environment or in R Statistical Software (Foundation for Statistical Computing, Austria). Data are presented as median ± median absolute deviation (MAD). Data were tested for significant differences (*P<0.05, **P<0.01 and ***P<0.001) using non-parametric Wilcoxon rank sum test for unpaired and Wilcoxon signed rank test for paired data or Kruskal-Wallis test with Bonferroni corrected post hoc analysis. Nested data were analyzed with linear mixed-effect models considering within animal variance with Turkey multi comparison correction for post hoc analysis. More information about statistic results are provided in Supplementary Tab. 1.

Supplementary figures

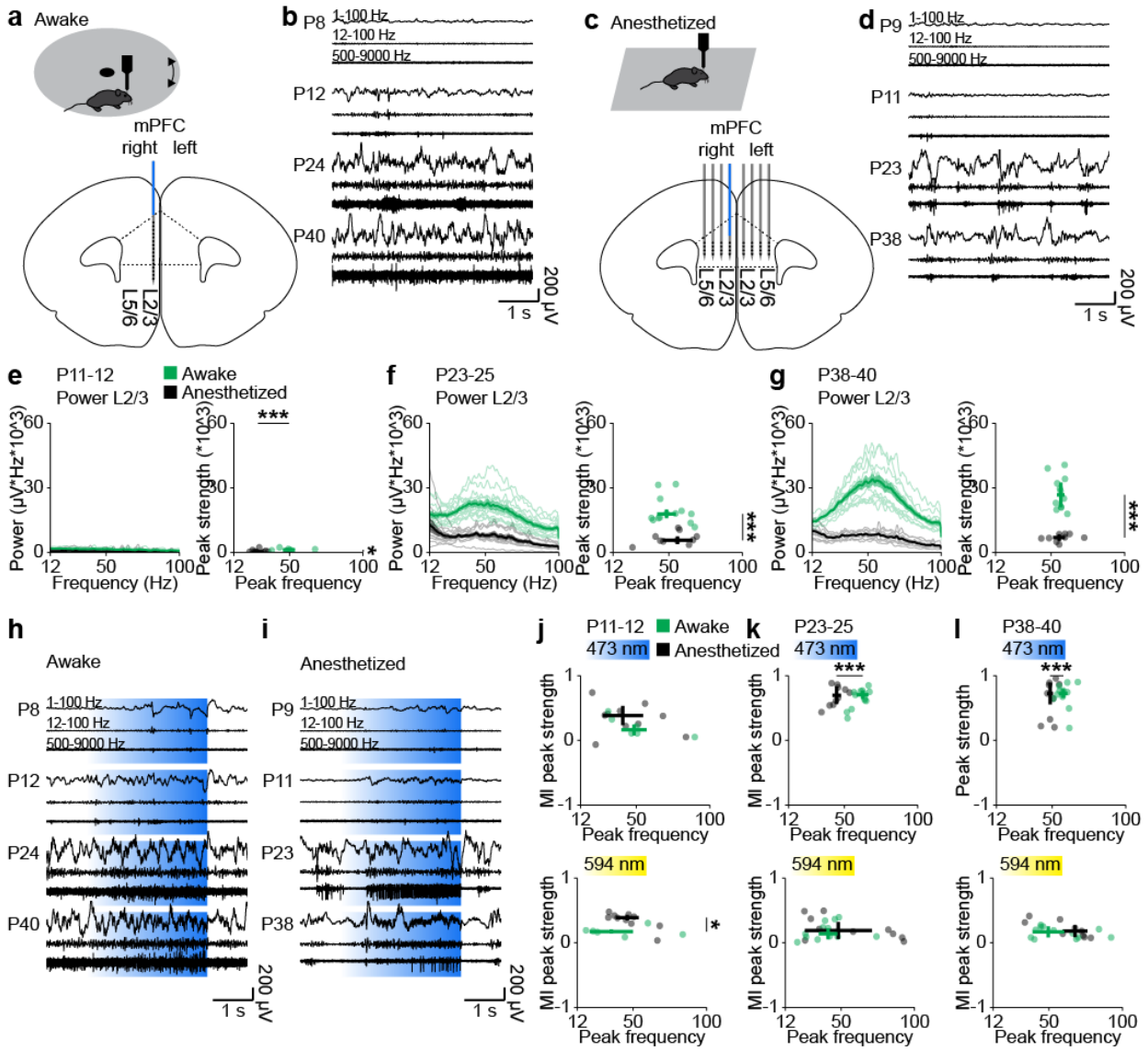

Supplementary Fig.1 (related to Fig. 1). Spontaneous and L2/3-driven activity in awake and anesthetized mice across development. (**a**) Setup for recordings from awake head-fixed mice on a spinning disc with one shank 1x16 electrode in L2/3. (**b**) Example LFPs from mPFC of non-anesthetized mice at different ages. (**c**) Setup for recordings from anesthetized head-fixed mice with four shank 4x4 electrode. (**d**) Example LFPs from mPFC of anesthetized mice at different ages. (**e**) Left, average power spectra of prefrontal activity for awake (n=6, 6 recordings) and anesthetized (n=10) P11-12 mice. Right, scatter plot displaying corresponding peak strength as a function of peak frequency. (**f**) Same as (e) for P23-25 mice (awake n=5, 13 recordings;

anesthetized n=10). (**g**) Same as (e) for P38-40 mice (awake n=5, 12 recordings; anesthetized n=9). (**h**) Example prefrontal LFPs driven by ramp light stimulation of L2/3 pyramidal neurons in non-anesthetized mice at different ages. (**i**) Example prefrontal LFPs driven by ramp light stimulation of L2/3 pyramidal neurons in anesthetized mice at different ages. (**j**) Scatter plots displaying peak strength as a function of peak frequency for the MI of power spectra during-to-before stimulation (ramp, 473 nm or 594 nm) in the mPFC of awake (n=6, 6 recordings) and anesthetized (n=10) P11-12 mice. (**k**) Same as (j) for P23-25 mice (awake n=5, 13 recordings; anesthetized n=10). (**l**) Same as (j) for P38-40 mice (awake n=5, 12 recordings; anesthetized n=9). *P<0.05, **P<0.01 and ***P<0.001. See Supplementary Tab. 1 for detailed information on statistics. Average data is presented as median ± MAD.

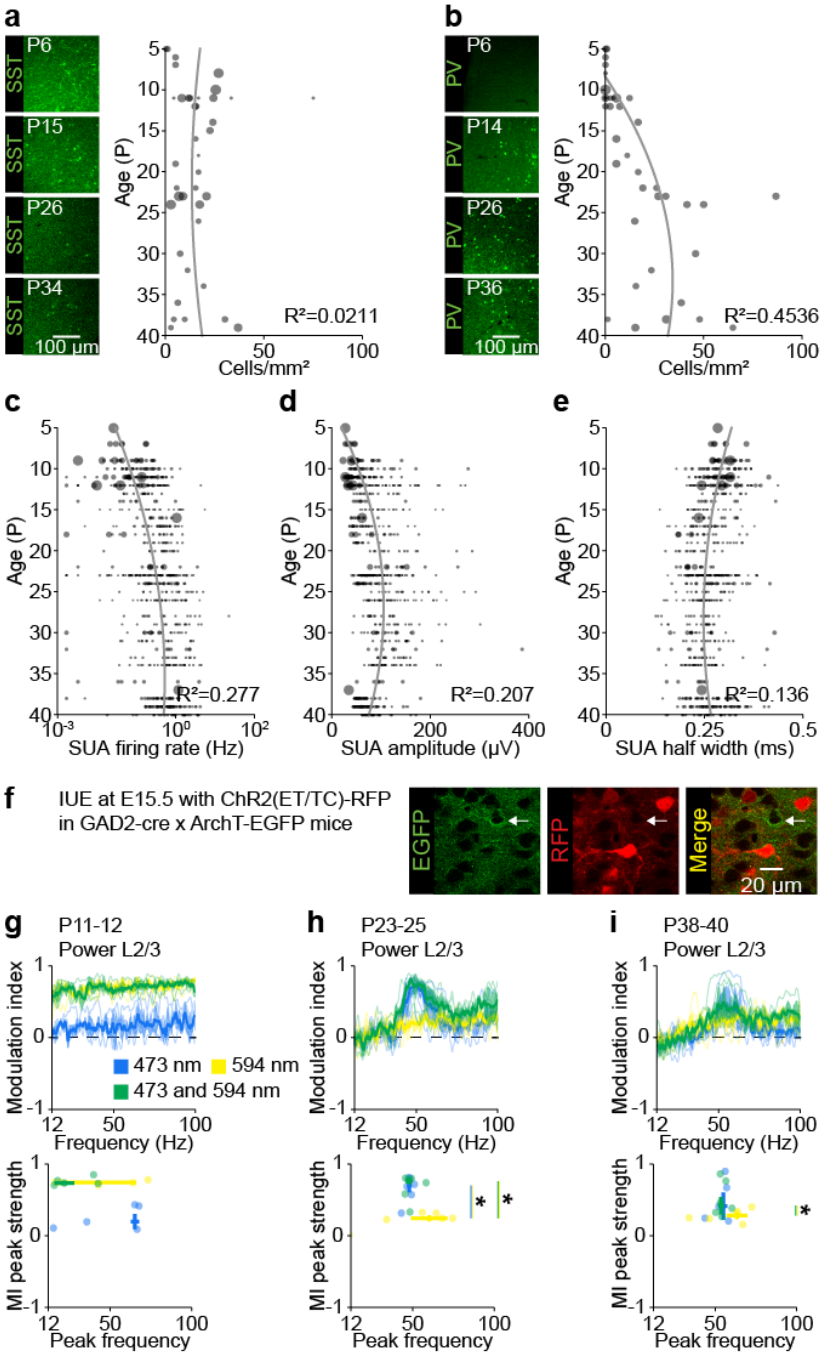

Supplementary Fig.2 (related to Fig. 1). Neurochemical identity and firing patterns in PFC across development. (**a**) Left, examples of SST immunostaining of prefrontal neurons from P6, P15, P26, and P34 mice. Right, scatter plot displaying the density of SST-immunopositive neurons in the mPFC of P5-40 mice (n=39). (**b**) Same for PV-immunopositive neurons (n=38). (**c**) Scatter plot displaying prefrontal SUA firing rate for P5-40 mice (806 units of 71 mice). (**d**) Same for SUA amplitude. (**e**) Same for unit half width. (**f**) Example of EGFP-positive (arrow) and RFP-positive cells showing no overlap

in expression. (**g**) Top, MI of power spectra during-to-before stimulation (ramp, 473 nm) of L2/3 pyramidal neurons (ramp, 473 nm), inhibition of interneurons (square pulse, 594 nm) or a combination of both in the mPFC of P11-12 mice (n=5). Bottom, scatter plot displaying corresponding peak strength as a function of peak frequency. (**h**) Same as (g) for P23-25 mice (n=6). (**i**) Same as (g) for P38-40 mice (n=6). *P<0.05, **P<0.01 and ***P<0.001. See Supplementary Tab. 1 for detailed information on statistics. Average data is presented as median ± MAD.

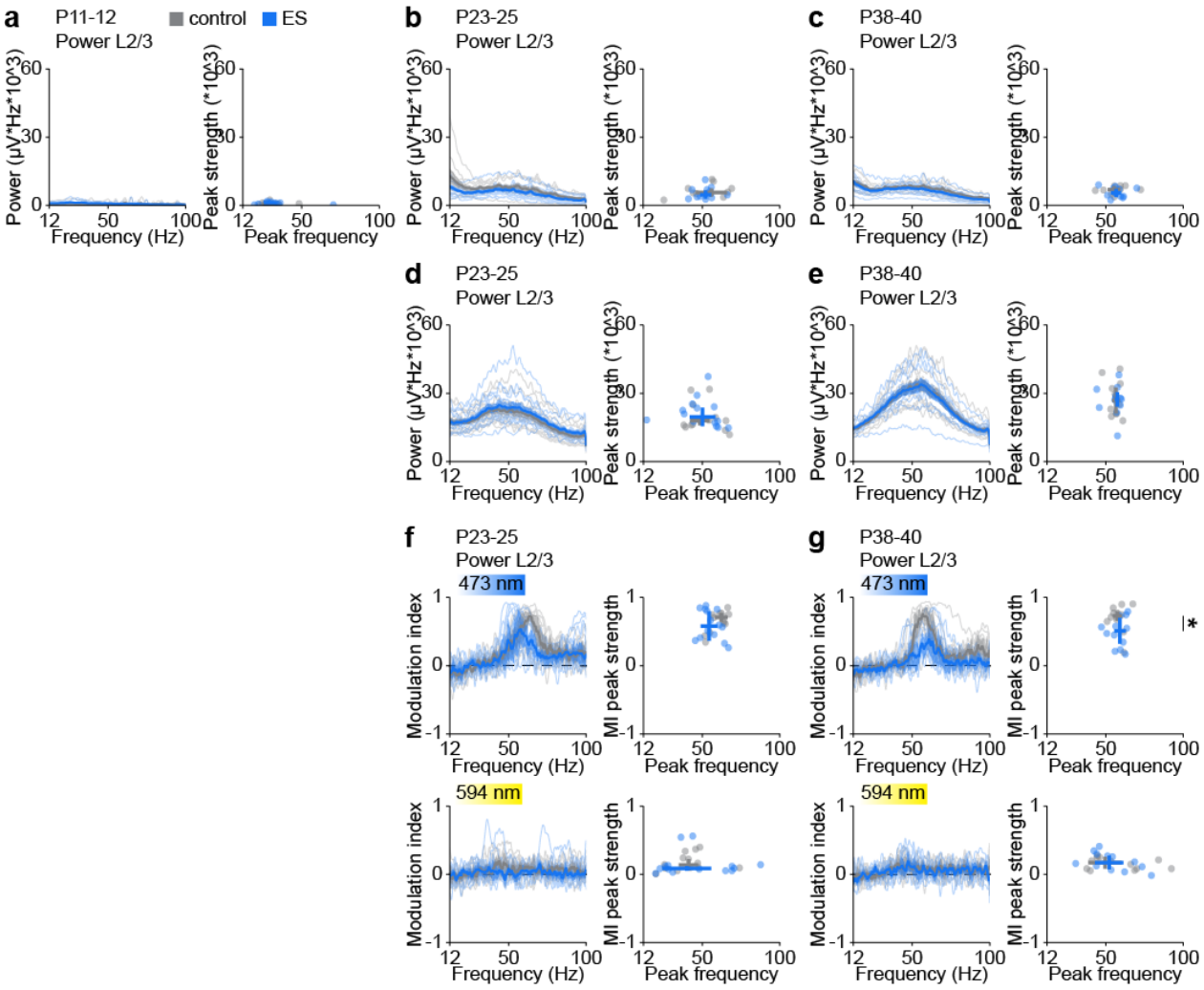

Supplementary Fig.3 (related to Fig. 3). ES effects on spontaneous and L2/3 pyramidal neuron-driven activity in anesthetized and awake head-fixed mice across development. (**a**) Left, average power spectra of spontaneous mPFC activity for anesthetized head-fixed P11-12 control (n=10) and ES mice (n=10). Right, scatter plot displaying corresponding peak strength as a function of peak frequency. (**b**) Same as (a) for P23-25 mice (control n=10, ES n=11). (**c**) Same as (a) for P38-40 mice (control n=9, ES n=12). (**d**) Same as (b) for awake head-fixed control (n=6, 13 recordings) and ES mice (n=5, 14 recordings) on a spinning disc. (**e**) Same as (c) for awake head-fixed control (n=5, 12 recordings) and ES mice (n=5, 12 recordings) on a spinning disc. (**f**) Top left, MI of power spectra during-to-before stimulation (ramp, 473 nm) of L2/3 pyramidal neurons in the mPFC of P23-25 awake control (n=6, 13 recordings) and ES mice (n=5, 14 recordings). Top right, scatter plot displaying corresponding peak strength

as a function of peak frequency. Bottom, same as top for control stimulation (ramp, 594 nm) (**g**) Same as (f) for P38-40 mice (control n=5, 12 recordings; ES n=5, 12 recordings). *P<0.05, **P<0.01 and ***P<0.001. See Supplementary Tab. 1 for detailed information on statistics. Average data is presented as median ± MAD.

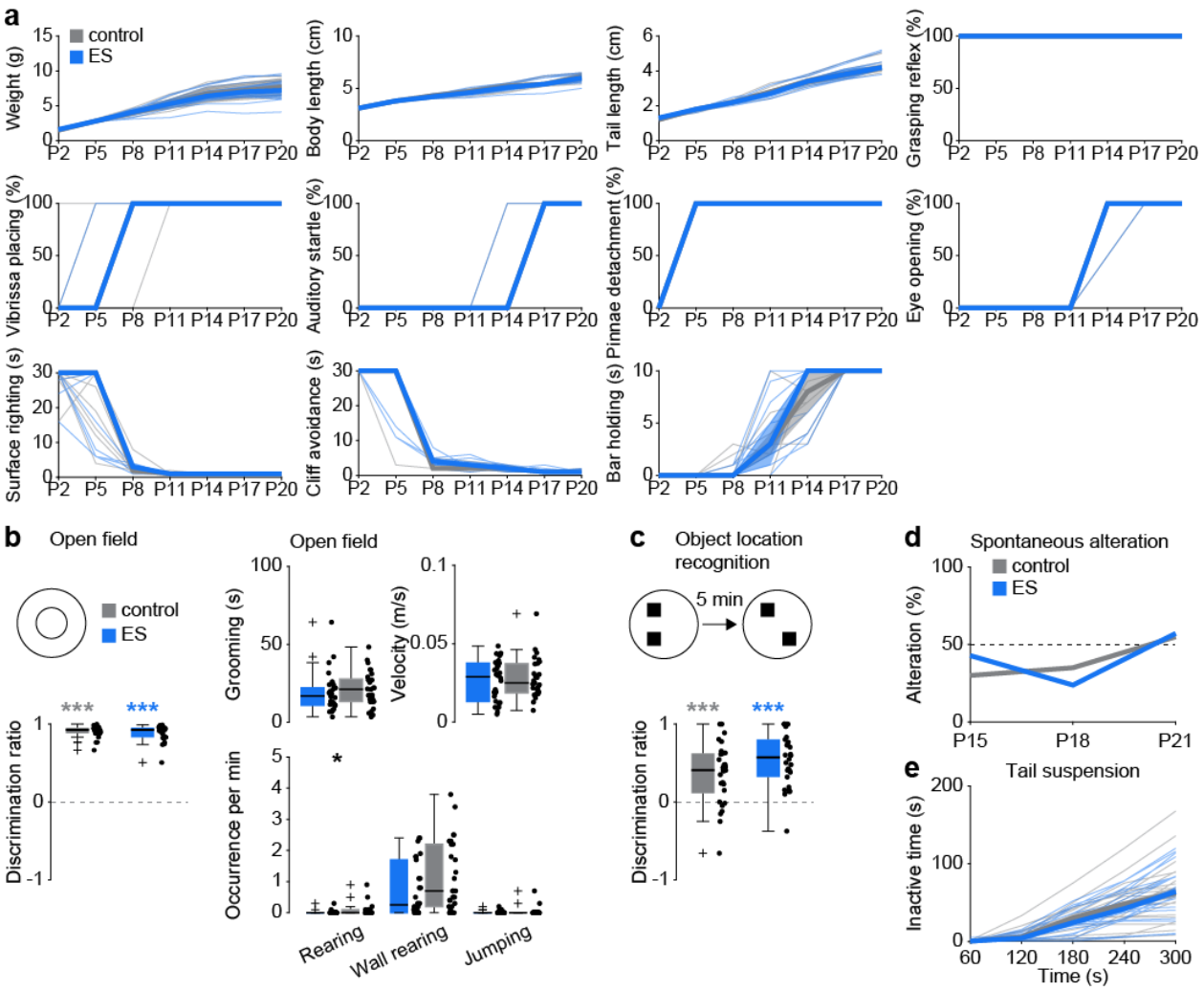

Supplementary Fig.4 (related to Fig. 4). Developmental milestones and behavioral performance after ES of L2/3 pyramidal neurons in the mPFC. (**a**) Age dependence of developmental milestones for control (n=11) and ES mice (n=11). (**b**) Left, schematic of open field task (top) and discrimination ratio of time spent in border-to-center in an open field (bottom). Right, behavioral quantification during exploration averaged for P16 control (n=28) and ES mice (n=30). (**c**) Top, schematic of object location recognition task. Bottom, discrimination ratio of interaction time with an object in a novel-to-familiar location averaged for P18 control (n=28) and ES mice (n=30). (**d**) Spontaneous alteration in t-maze test for control (n=19) and ES mice (n=21) at P15, 18 and 21. (**e**) Tail suspension test for P21 control (n=19) and ES mice (n=21). *P<0.05, **P<0.01 and ***P<0.001. See Supplementary Tab. 1 for detailed information on statistics. Average data is presented as median ± MAD.